

# An integral equation solution for the steady-state current at a periodic array of surface microelectrodes

S.K. Lucas, School of Mathematics, University of South Australia,  
The Levels SA 5095, AUSTRALIA

H.A. Stone, Division of Applied Sciences, Harvard University, Cam-  
bridge MA 02138, U.S.A.

R. Sipicic, Department of Mathematics, Massachusetts Institute of  
Technology, Cambridge MA 02139, U.S.A.

Submitted September 1995, Revised July 1996,  
to *SIAM Journal on Applied Mathematics*

## Abstract

An integral equation approach is developed for the problem of determining the steady-state current to a periodic array of microelectrodes imbedded in an otherwise insulating plane. The formulation accounts for both surface electrode and bulk fluid reactions, and evaluates the Green's functions for periodic systems using convergence acceleration techniques. Numerical results are presented for disc-shaped microelectrodes at the center of rectangular periodic cells for a large range of dimensionless surface and bulk reaction rates and periodic cell sizes.

## Keywords:

electrochemistry, reaction-diffusion, boundary integral method, microelectrode arrays

## Subject Classifications:

92E20 - Chemistry, Reactions

65R20 - Numerical analysis, Integral equations

65B99 - Acceleration of convergence, Other

## Abbreviated title:

Current at an array of microelectrodes

# 1 Introduction

Mass transport coupling diffusion, surface and/or bulk chemical reactions, and species migration in external fields occurs in a wide variety of physical situations, including electrochemistry, catalysis, corrosion, colloidal suspensions, and protein binding. Such transport processes are frequently controlled by surface chemical reactions or by charge distributed along the surfaces bounding the fluid. In general, the bounding surfaces are heterogeneous and so surface properties (e.g. reactivity) vary. For example, electrochemical devices consisting of arrays of microelectrodes (Wightman and Wipf [35], Mallouk [19]) or catalysis along heterogeneous surfaces (Kuan *et al.* [16, 17]) have in common the geometric feature that surface chemical reactions occur on many distributed regions, or patches, on an otherwise unreactive substrate. Although mass transfer to an isolated surface patch has been studied for a variety of surface geometries (e.g. strips, hemispheres, discs, and rings), the case of multiple active surface sites has received much less attention. This paper addresses this question by studying reaction-diffusion problems in a stationary fluid bounded by a plane that is covered by a periodic array of circular reactive sites.

The electrochemical literature contains many studies of the current at an electrode of various given shapes. The small size of microelectrodes typically leads to situations where transients are short-lived and so the accompanying mass transport may be treated as steady state. Isolated microelectrodes in the shape of hemispheres (Oldham and Zoski [23]), discs (Aoki *et al.* [2], Bond *et al.* [6], Phillips [24, 25], Bender and Stone [5]) and rings (Fleischmann *et al.* [9, 10], Szabo [33], Phillips and Stone [27]) have been analyzed most frequently, mostly for the case of bulk diffusion with surface chemical reaction (the Laplace equation), but also for bulk diffusion with surface chemical reaction and bulk species regeneration by chemical reaction (the modified Helmholtz equation).

Recent electrochemical applications utilize microelectrode arrays (Wightman and Wipf [35]). In general, it is of interest to determine an effective rate constant for the heterogeneous surface which depends on both the reactivity of active sites as well as their surface coverage. Theoretical analysis of such arrays must treat the interaction of the different surface reactive sites and, perhaps not surprisingly, theoretical analyses have been limited to the case of small fractional coverages of a finite surface (Phillips [26]) and numerical results for a small number of electrodes on an infinite surface (Fransaer *et al.* [11]). Included in [26] are several references to problems dealing with microelectrode arrays of infinite extent, including studies by Reller *et al.* [30] and Scharifker [32], who investigate time-dependent currents, though since diffusion with no regeneration within the fluid is considered, the steady state result is zero current. In addition, in [30] and [32], a periodic array geometry is approximated by solving instead the problem of a disc electrode surrounded by an insulating annulus. We also note that mass transport problems related to the present investigation of multiple reactive surface sites naturally arise in the modelling of catalytic surfaces (Kuan *et al.* [16, 17]), the double layer forces between surfaces with a heterogeneous charge distribution (Miklavic *et al.* [20]), multi-particle Ostwald ripening (Voorhees and Glicksman [34]), and protein binding (Balgi *et al.* [3]). Related mathematical formulations also arise in studies of the effective conductivity of a suspension of particles of one conductivity dispersed within a matrix of different conductivity (Bonnetcaze and Brady [7]), and acoustic properties of

bubbly liquids (Sangani and Sureshkumar [31]), where regular three-dimensional arrays are analyzed.

A mathematical model of the typical reaction-diffusion situation characteristic of the microelectrode geometry is to consider a distribution of reaction sites (e.g. discs) on an otherwise unreactive plane boundary underlying a stagnant fluid. We shall consider here the case of periodic surface arrays so that the transport problem is also periodic. Since this geometry is three-dimensional, we have a mathematical problem involving a two-dimensional periodicity embedded within three-dimensional space. The basic equations and their solution in terms of an integral equation are given in Section 2, along with three forms of the Green's function. A description of the numerical methods of solution is given in Section 3, and representative numerical results are presented in Section 4.

## 2 Formulation

### 2.1 Problem Statement

Consider a periodic array of circular disc-shaped microelectrodes distributed over an otherwise insulating boundary as illustrated in Figure 1. An electrolytic solution fills the entire volume above the plane, and we are interested in calculating the steady-state current to the surface due to oxidation-reduction processes that occur on the surface of the electrodes; effects due to possible chemical regeneration in the bulk are also considered. The flux of the given chemical to the electrode is proportional to the measured electrode current, and so we seek a solution for the concentration flux of the chemical species. We assume that there is no fluid motion, so the usual reaction-diffusion equations apply as in the literature cited above.

The electrode surfaces are denoted  $S_E$  and the insulating planar region is denoted  $S_P$ . We choose coordinates such that the insulating plane is at  $z = 0$ , and the electrolytic solution fills the volume  $z > 0$ . Following Phillips [24, 25] (see also Bender and Stone [5]), the steady state reaction-diffusion problem may be written in the dimensionless form

$$\nabla^2 \phi = \alpha^2 \phi \quad \text{where} \quad \begin{cases} \phi = 1 + \frac{1}{K} \frac{\partial \phi}{\partial z} & \text{on } z = 0, \mathbf{r} \in S_E, \\ \frac{\partial \phi}{\partial z} = 0 & \text{on } z = 0, \mathbf{r} \in S_P, \\ \phi \rightarrow 0 & \text{as } z \rightarrow \infty, \end{cases} \quad (1)$$

where  $\phi(\mathbf{r})$  is the dimensionless concentration in the fluid,  $\alpha^2$  is a constant representing the ratio of bulk species regeneration relative to diffusion,  $K$  is a constant representing the ratio of surface reaction rate at the electrode surface relative to diffusion in the bulk, and  $\mathbf{r}$  denotes the position vector. A large value of  $\alpha$  indicates a large bulk regeneration, and so most activity will take place near the electrode, while a small value of  $\alpha$  indicates diffusion becoming more important, as reactants must be transported inwards from infinity rather than being regenerated near the electrode. An infinite value for  $K$  is the limit in which reaction takes place instantaneously at the electrode. Smaller values of

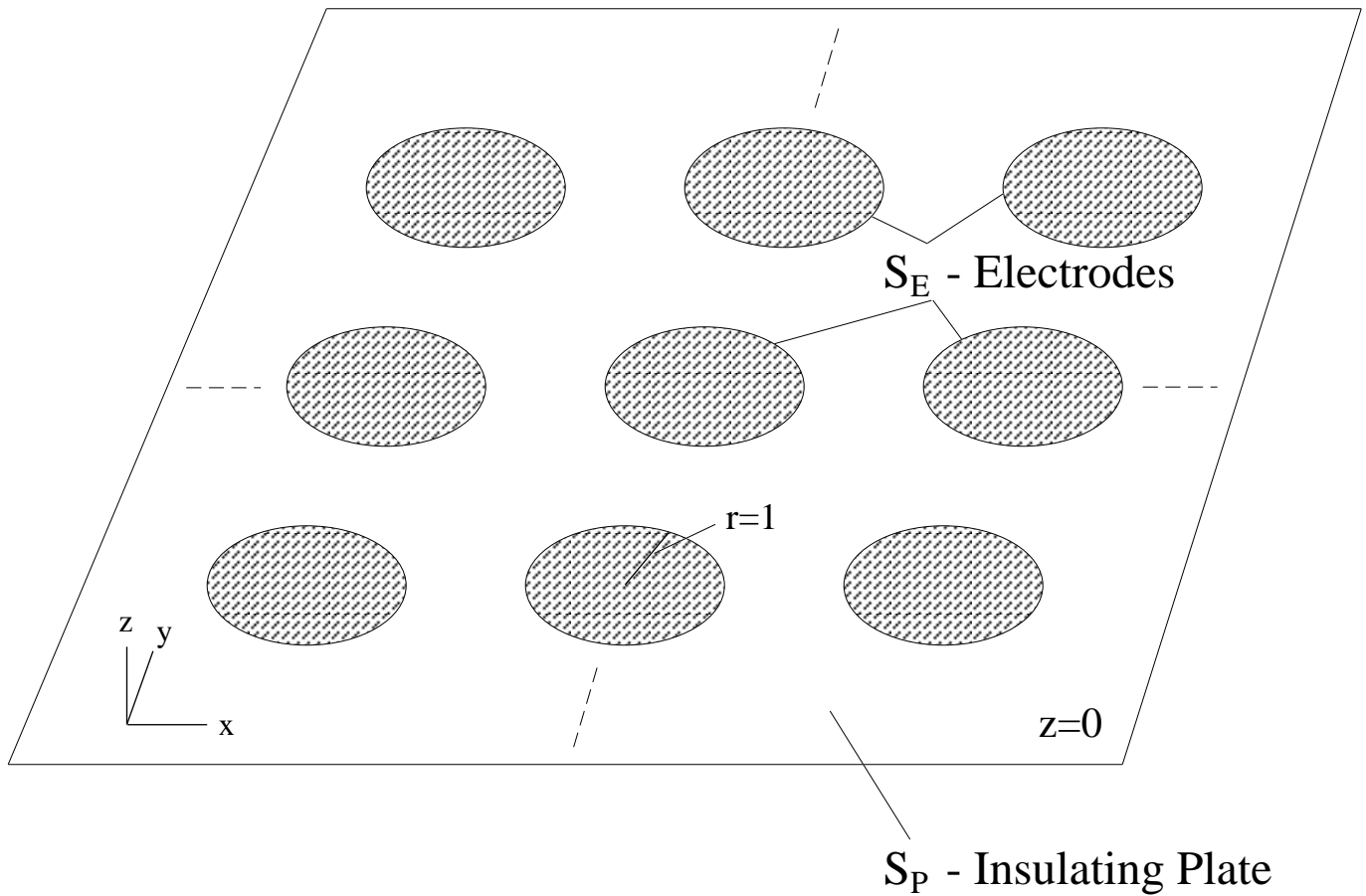


Figure 1: The periodic array of microelectrodes on an insulating plane.

$K$  indicate a slower surface reaction at the electrode. In the limit  $K = 0$ , no surface reaction takes place and the solution is  $\phi = 0$  everywhere (the first boundary condition of (1) reduces to  $\partial\phi/\partial z = 0$  on  $z = 0$ ,  $\mathbf{r} \in S_E$ ). Equation (1) can be recognized as the modified Helmholtz equation with mixed boundary conditions.

Here, we shall assume that the surface consists of rectangular periodic cells of size  $2l_1 \times 2l_2$ , with circular microelectrodes of radius one centered within the periodic cells, as shown in Figure 2. Due to the periodicity, we shall only need to determine the solution within a single cell. Rather than calculate the concentration  $\phi$  directly, we are more interested in the flux  $\partial\phi/\partial z$  on the plane  $z = 0$ . Once the flux distribution has been calculated, the total dimensionless flux to a single electrode follows from

$$\text{Total Flux per electrode} = - \int_{S_E} \frac{\partial\phi}{\partial z} dS, \quad (2)$$

which is proportional to the measured current through the electrode. Since we are only interested in finding the flux distribution over the electrode, the domain of application of (1) is the infinite half-space, and, additionally, as the boundary value problem is linear, an integral equation approach is ideal. This mathematical approach is common, although some of the analytical details necessary to treat the periodic surface condition and numerical details to represent the flux accurately require some care.

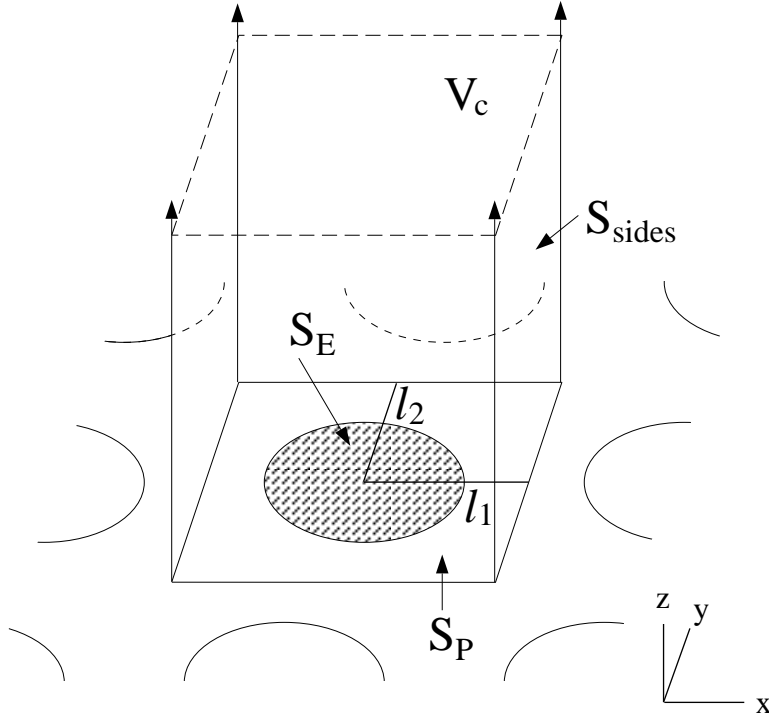


Figure 2: Geometry of the volume above a periodic cell for the problem.

## 2.2 Integral Equation Derivation

Due to the periodic nature of the problem, we have that  $\phi(\mathbf{r}) = \phi(\mathbf{r} + \mathbf{r}_p)$ , where

$$\mathbf{r}_p = (2l_1m_1, 2l_2m_2, 0), \quad m_1, m_2 = 0, \pm 1, \pm 2, \dots \quad (3)$$

is the periodic vector. Rather than solving for  $\phi$  throughout the entire volume, we may treat instead the volume above a single periodic cell (see Figure 2), with volume  $V_c$  and boundary  $S_c = S_E \cup S_P \cup S_\infty \cup S_{sides}$ . The surface  $S_\infty$  is the ‘cap’ of the volume at  $z = \infty$ . Applying Green’s theorem to  $V_c$  gives

$$\int_{V_c} (G\nabla^2\phi - \phi\nabla^2G) dV = \int_{S_c} \left( G\frac{\partial\phi}{\partial n} - \phi\frac{\partial G}{\partial n} \right) dS, \quad (4)$$

where  $G$  is the appropriate periodic Green’s function for the problem. Provided  $\alpha > 0$ , it can be shown that the surface integrals over  $S_\infty$  vanish. Also, periodicity ensures no net flux in  $\phi$  or  $G$  over the surfaces  $S_{sides}$ .

We require a spatially periodic Green’s function that satisfies

$$G(\mathbf{r} - \mathbf{r}_0) = G(\mathbf{r} - \mathbf{r}_0 - \mathbf{r}_p), \quad m = 0, \pm 1, \pm 2, \dots \quad (5)$$

where  $\mathbf{r}$  is the position vector,  $\mathbf{r}_0$  is the position of the delta function in the equation for the Green’s function, and  $\mathbf{r}_p$  is given in (3). This Green’s function can be interpreted as the response at  $\mathbf{r}$  due to a forcing at the lattice points  $\mathbf{r}_0 + \mathbf{r}_p$ . Writing  $\mathbf{R} = \mathbf{r} - \mathbf{r}_0$ , we

have that the Green's function must satisfy

$$\nabla_{\mathbf{r}}^2 G(\mathbf{R}) = \alpha^2 G(\mathbf{R}) + \sum_{m_1=-\infty}^{\infty} \sum_{m_2=-\infty}^{\infty} \delta(\mathbf{R} - \mathbf{r}_p) \quad \text{with } G \rightarrow 0 \text{ as } |R_3| \rightarrow \infty, \quad (6)$$

where the Laplacian operator is with respect to the variable  $\mathbf{r}$ , and  $R_3$  is the  $z$ -component of  $\mathbf{R}$ .

Given an appropriate solution of (6), which is described in detail in section 2.3, the Green's function is substituted into (4), and the source point  $\mathbf{r}_0$  moved to the boundary (as is standard in applications of the boundary integral method, e.g. Brebbia *et al.* [8]). Thus, we arrive at

$$-\frac{1}{2}\phi(\mathbf{r}_0) = \int_{S_E \cup S_P} \left( G(\mathbf{R}) \frac{\partial \phi}{\partial n}(\mathbf{r}) - \phi(\mathbf{r}) \frac{\partial G}{\partial n}(\mathbf{R}) \right) dS(\mathbf{r}), \quad \mathbf{r}_0 \in S_E \cup S_P. \quad (7)$$

Since the surface  $S_E \cup S_P$  is that part of the periodic cell boundary in the plane  $z = 0$ , we have that  $\partial/\partial n \equiv -\partial/\partial z$ , and it may be shown that  $\partial G/\partial z = 0$  when both  $\mathbf{r}$  and  $\mathbf{r}_0$  are on the plane  $z = 0$  ( $R_3 = 0$ ). Thus, (7) reduces to

$$\frac{1}{2}\phi(\mathbf{r}_0) = \int_{S_E \cup S_P} G(\mathbf{R}) \frac{\partial \phi}{\partial z}(\mathbf{r}) dS(\mathbf{r}). \quad (8)$$

Finally, applying the boundary conditions on  $S_E$  and  $S_P$  from (1), we obtain the integral formulation for the flux of  $\phi$  through the electrode as

$$1 + \frac{1}{K}\phi'(\mathbf{r}_0) = \int_{S_E} 2G(\mathbf{r} - \mathbf{r}_0)\phi'(\mathbf{r}) dS(\mathbf{r}), \quad \mathbf{r}_0 \in S_E, \quad (9)$$

where we have written  $\phi'$  for  $\partial\phi/\partial z$ . We note that  $\mathbf{r}_0$  need only be taken over the surface of the electrode  $S_E$ , where  $S_E$  is the disc of radius one centered at the origin on the plane  $z = 0$ . The specific geometry of the periodic surface (the parameters  $l_1$  and  $l_2$ ) enter the problem through the Green's function  $G$  as described in the next section.

## 2.3 The Periodic Green's Function

To find the Green's function, we first note that  $\mathbf{r}_0$  is fixed as the position  $\mathbf{r}$  is varied, so  $\nabla_{\mathbf{r}}^2 \equiv \nabla_{\mathbf{R}}^2$ , and (6) can be written as

$$\nabla_{\mathbf{R}}^2 G(\mathbf{R}) = \alpha^2 G(\mathbf{R}) + \delta(R_3) \sum_m \delta(R_1 - 2l_1 m_1) \delta(R_2 - 2m_2 l_2), \quad (10)$$

where we have used the definition of  $\mathbf{r}_p$  and written  $\sum_m$  to represent the infinite double summation over  $m_1$  and  $m_2$ . To solve (10), we make use of two-dimensional Fourier transforms  $\mathcal{F}_2$  in  $(R_1, R_2)$ , as defined in Nijboer and De Wette [22]:

$$\left. \begin{aligned} \mathcal{F}_2 f(R_1, R_2) &= \hat{f}(k_1, k_2) = \int_{-\infty}^{\infty} \int_{-\infty}^{\infty} e^{2\pi i(k_1 R_1 + k_2 R_2)} f(R_1, R_2) dR_2 dR_1, \\ \mathcal{F}_2^{-1} \{ \hat{f}(k_1, k_2) \} &= f(R_1, R_2) = \int_{-\infty}^{\infty} \int_{-\infty}^{\infty} e^{-2\pi i(k_1 R_1 + k_2 R_2)} \hat{f}(k_1, k_2) dk_2 dk_1. \end{aligned} \right\} \quad (11)$$

Taking the two-dimensional Fourier transform of (10), and using the standard result (Barton [4]) that

$$\sum_m \delta(x_1 - m_1 L_1) \delta(x_2 - m_2 L_2) = \frac{1}{L_1 L_2} \sum_m e^{2\pi i \left( \frac{m_1 x_1}{L_1} + \frac{m_2 x_2}{L_2} \right)}, \quad (12)$$

we obtain the equation

$$\frac{\partial^2 \hat{G}}{\partial R_3^2} - \left( 4\pi^2(k_1^2 + k_2^2) + \alpha^2 \right) \hat{G} = \frac{\delta(R_3)}{4l_1 l_2} \sum_m \delta \left( k_1 - \frac{m_1}{2l_1} \right) \delta \left( k_2 - \frac{m_2}{2l_2} \right), \quad (13)$$

which has the solution

$$\hat{G} = -\frac{e^{-|R_3| \sqrt{4\pi^2(k_1^2 + k_2^2) + \alpha^2}}}{8l_1 l_2 \sqrt{4\pi^2(k_1^2 + k_2^2) + \alpha^2}} \sum_m \delta \left( k_1 - \frac{m_1}{2l_1} \right) \delta \left( k_2 - \frac{m_2}{2l_2} \right). \quad (14)$$

Using the inverse transform, we obtain the Green's function

$$G(\mathbf{R}) = -\sum_m \frac{\exp \left\{ -\pi i \left( \frac{m_1 R_1}{l_1} + \frac{m_2 R_2}{l_2} \right) - |R_3| \sqrt{\pi^2 \left[ \left( \frac{m_1}{l_1} \right)^2 + \left( \frac{m_2}{l_2} \right)^2 \right] + \alpha^2} \right\}}{8l_1 l_2 \sqrt{\pi^2 \left[ \left( \frac{m_1}{l_1} \right)^2 + \left( \frac{m_2}{l_2} \right)^2 \right] + \alpha^2}}. \quad (15)$$

Note that in (9), both  $\mathbf{r}$  and  $\mathbf{r}_0$  lie on the plane  $z = 0$ , so that  $R_3 = 0$ , which is a useful simplification for some of the mathematical manipulations that follow.

## 2.4 Accelerating the Convergence Rate of the Green's Function

The form of the Green's function given in (15) is computationally inefficient because the convergence rate is very slow when  $|R_3|$  is small or zero, and a large number of terms are required to calculate (15) to even a few figures of accuracy. A more useful form of the Green's function can be obtained using various acceleration techniques such as the Poisson summation formula or the method of Ewald. We mention at this point that the double summation over  $m_1$  and  $m_2$  is calculated by starting with the term  $m_1 = m_2 = 0$  and adding successive layers corresponding to  $|m_1| + |m_2| = j$ ,  $j = 1, 2, \dots$ . Geometrically, this ensures that the partial sum is that of a square of terms surrounding  $m_1 = m_2 = 0$ .

### 2.4.1 The Poisson Summation Formula

The principle of the Poisson summation formula is that the Fourier transform of a smooth function approaches zero more rapidly than the original function. The Poisson summation formula in one dimension is clearly outlined in Barton [4], and the two-dimensional form can be constructed using the same procedure:

$$\sum_m F(\lambda_1 m_1, \lambda_2 m_2) = \frac{1}{\lambda_1 \lambda_2} \sum_m \int_{-\infty}^{\infty} \int_{-\infty}^{\infty} F(\xi_1, \xi_2) e^{2\pi i \left( \frac{m_1 \xi_1}{\lambda_1} + \frac{m_2 \xi_2}{\lambda_2} \right)} d\xi_2 d\xi_1. \quad (16)$$

Applying (16) to (15), we find

$$G(\mathbf{R}) = -\frac{1}{8} \sum_m \int_{-\infty}^{\infty} \int_{-\infty}^{\infty} \frac{e^{-\pi i(\xi_1 k_1 + \xi_2 k_2) - |R_3| \sqrt{\pi^2(\xi_1^2 + \xi_2^2) + \alpha^2}}}{\sqrt{\pi^2(\xi_1^2 + \xi_2^2) + \alpha^2}} d\xi_2 d\xi_1, \quad (17)$$

where  $(k_1, k_2) = (R_1 - 2l_1 m_1, R_2 - 2l_2 m_2)$ . Transforming to polar coordinates using  $\xi_1 = a \cos \theta$ ,  $\xi_2 = a \sin \theta$ , and  $k_1 = k \cos \varphi$ ,  $k_2 = k \sin \varphi$  with  $k^2 = (R_1 - 2l_1 m_1)^2 + (R_2 - 2l_2 m_2)^2$ , and using equation (3.915.2) from Gradshteyn and Ryzhik [12],

$$\int_0^\pi e^{i\beta \cos x} \cos(nx) dx = i^n \pi J_n(\beta), \quad (18)$$

we obtain

$$G(\mathbf{R}) = -\frac{\pi}{4} \sum_m \int_0^\infty \frac{a J_0(\pi k a)}{\sqrt{\pi^2 a^2 + \alpha^2}} e^{-|R_3| \sqrt{\pi^2 a^2 + \alpha^2}} da. \quad (19)$$

Applying the transform  $a^2 = \alpha^2(u^2 - 1)/\pi^2$ , and using equation (6.616.2) from Gradshteyn and Ryzhik [12] that

$$\int_1^\infty e^{-\alpha x} J_0(\beta \sqrt{x^2 - 1}) dx = \frac{1}{\sqrt{\alpha^2 + \beta^2}} e^{-\sqrt{\alpha^2 + \beta^2}}, \quad (20)$$

equation (19) becomes

$$\begin{aligned} G(\mathbf{R}) &= -\frac{1}{4\pi} \sum_m \frac{\exp\left[-\alpha \sqrt{R_3^2 + k^2}\right]}{\sqrt{k^2 + R_3^2}}, \\ &= -\frac{1}{4\pi} \sum_m \frac{\exp\left[-\alpha \sqrt{(R_1 - 2m_1 l_1)^2 + (R_2 - 2m_2 l_2)^2 + R_3^2}\right]}{\sqrt{(R_1 - 2m_1 l_1)^2 + (R_2 - 2m_2 l_2)^2 + R_3^2}}. \end{aligned} \quad (21)$$

From this exponential form of  $G(\mathbf{R})$ , it can be shown that  $\partial G/\partial z = 0$  when  $R_3 = 0$ , as was required in the derivation of (9).

The representation of the Green's function in (21) is the same as would be obtained by distributing the three-dimensional free-space Green's function for the modified Helmholtz equation

$$G(\mathbf{r} - \mathbf{r}_0) = -\frac{1}{4\pi} \frac{e^{-\alpha|\mathbf{r}-\mathbf{r}_0|}}{|\mathbf{r} - \mathbf{r}_0|} \quad (22)$$

over all the electrodes to deal with spatial periodicity. Of course, (22) could have been written down immediately, but it is useful to understand the steps (16-21) in order to apply the Ewald method to this problem.

While the exponential in the summation for  $G(\mathbf{R})$  in (21) ensures that its convergence is faster than for (15), the convergence rate can still be quite poor for small  $\alpha$ . In such cases, we will use the method of Ewald, which we now outline.

#### 2.4.2 The Method of Ewald

The method of Ewald is a technique for improving the convergence rates of slowly converging lattice sums. We assume  $R_3 = 0$  in the derivation that follows.

We wish to accelerate the convergence of

$$G(\mathbf{R}) = - \sum_m \frac{\exp \left[ -\pi i \left( \frac{m_1 R_1}{l_1} + \frac{m_2 R_2}{l_2} \right) \right]}{8l_1 l_2 \sqrt{\pi^2 \left\{ \left( \frac{m_1}{l_1} \right)^2 + \left( \frac{m_2}{l_2} \right)^2 \right\} + \alpha^2}}. \quad (23)$$

Using the fact that  $\operatorname{erf}(x) + \operatorname{erfc}(x) = 1$ , we rewrite (23) as

$$G(\mathbf{R}) = S_1 + S_2, \quad (24)$$

where

$$\begin{aligned} S_1 &= - \sum_m \frac{\exp \left[ -\pi i \left( \frac{m_1 R_1}{l_1} + \frac{m_2 R_2}{l_2} \right) \right] \operatorname{erfc} \left( c\sqrt{A} \right)}{8l_1 l_2 \sqrt{A}}, \\ S_2 &= - \sum_m \frac{\exp \left[ -\pi i \left( \frac{m_1 R_1}{l_1} + \frac{m_2 R_2}{l_2} \right) \right] \operatorname{erf} \left( c\sqrt{A} \right)}{8l_1 l_2 \sqrt{A}}, \end{aligned} \quad (25)$$

$A = \pi^2 \{ (m_1/l_1)^2 + (m_2/l_2)^2 \} + \alpha^2$ , and  $c$  is an arbitrary constant. Due to the nature of the complimentary error function, the sum  $S_1$  converges very quickly, but the rate of convergence of  $S_2$  is unchanged. The Ewald method as described in Nijboer and De Wette [22] accelerates the convergence of  $S_2$  by first converting the summation terms into integrals using properties of the delta function, and then applying the Fourier convolution theorem to accelerate convergence. However, the same final result can be obtained more easily by applying the two-dimensional Poisson's summation formula to  $S_2$ . Identifying  $\lambda_i = 1/l_i$ , and applying (16) to (25b), we find that

$$S_2 = - \sum_m \frac{1}{4} \int_{-\infty}^{\infty} \int_{-\infty}^{\infty} e^{-\pi i(k_1 \xi_1 + k_2 \xi_2)} \frac{\operatorname{erf} \left( c\sqrt{\pi^2(\xi_1^2 + \xi_2^2) + \alpha^2} \right)}{\sqrt{\pi^2(\xi_1^2 + \xi_2^2) + \alpha^2}} d\xi_2 d\xi_1, \quad (26)$$

where  $(k_1, k_2) = (R_1 - 2m_1 l_1, R_2 - 2m_2 l_2)$ . Since  $d(\operatorname{erf}(x))/dx = 2 \exp(-x^2)/\sqrt{\pi}$ , we may take the derivative of  $S_2$  with respect to  $c$  to show that

$$\frac{dS_2}{dc} = - \sum_m \frac{1}{2c^2 \pi^{3/2}} e^{-\alpha^2 c^2 - \frac{k^2}{4c^2}}, \quad (27)$$

where  $k^2 = k_1^2 + k_2^2$ , and we have (Gradshteyn and Ryzhik [12], equation (3.896.4))

$$\int_0^{\infty} e^{-\beta x^2} \cos(bx) dx = \frac{1}{2} \sqrt{\frac{\pi}{\beta}} e^{-\frac{b^2}{4\beta}}, \quad \operatorname{Re}(\beta) > 0. \quad (28)$$

Now, integrating (27) leads to

$$S_2 = - \sum_m \frac{1}{4\pi k} \left[ e^{k\alpha} \operatorname{erfc} \left( \frac{k}{2c} + \alpha c \right) + e^{-k\alpha} \operatorname{erfc} \left( \frac{k}{2c} - \alpha c \right) \right], \quad (29)$$

where we have used (Abramowitz and Stegun [1], equation (7.4.33))

$$\int e^{-a^2 x^2 - \frac{b^2}{x^2}} dx = \frac{\sqrt{\pi}}{4a} \left[ e^{2ab} \operatorname{erf} \left( ax + \frac{b}{x} \right) + e^{-2ab} \operatorname{erf} \left( ax - \frac{b}{x} \right) \right] + C. \quad (30)$$

Thus, we have the final result that when  $R_3 = 0$ ,

$$G(\mathbf{R}) = -\frac{1}{4l_1l_2} \sum_m e^{\pi i \left( \frac{m_1 R_1}{l_1} + \frac{m_2 R_2}{l_2} \right)} \frac{\operatorname{erfc}(c\sqrt{A})}{\sqrt{A}} - \frac{1}{4\pi} \sum_m \frac{1}{k} \left[ e^{k\alpha} \operatorname{erfc} \left( \frac{k}{2c} + \alpha c \right) + e^{-k\alpha} \operatorname{erfc} \left( \frac{k}{2c} - \alpha c \right) \right], \quad (31)$$

where

$$k = \sqrt{(R_1 - 2l_1m_1)^2 + (R_2 - 2l_2m_2)^2} \quad \text{and} \quad A = \pi^2 \left\{ \left( \frac{m_1}{l_1} \right)^2 + \left( \frac{m_2}{l_2} \right)^2 \right\} + \alpha^2. \quad (32)$$

The arbitrary parameter  $c$  is chosen to obtain the best convergence for  $G(\mathbf{R})$ . Since  $\operatorname{erfc}(x) = O(e^{-x^2})$  for  $x \gg 1$ , we can balance the convergence rates of the complimentary error function terms in (31) to arrive at the estimate

$$c = \sqrt{\frac{l_1 l_2}{\pi}}. \quad (33)$$

### 2.4.3 Choosing an Acceleration Technique

The convergence rate of  $G(\mathbf{R})$  depends on  $\alpha$ , and the geometric parameters  $l_1$  and  $l_2$ . While the convergence rate for  $G(\mathbf{R})$  using the Ewald sum (31) has been found to be relatively insensitive to the value of  $\alpha$ , and the convergence rate of the Ewald sum is  $O(e^{-m^2})$  compared to the  $O(e^{-m})$  rate of the Poisson sum (21), it is not an automatic choice to always use the Ewald result rather than the Poisson sum. Each term of the Ewald sum requires the calculation of three complimentary error functions, while the Poisson sum terms only require evaluation of a single exponential function. Thus from a computational view, the Poisson sum may be more efficient than the Ewald sum.

Our initial choice for calculating the complimentary error function was the routine `derfc()` from the IMSL numerical package [36]. However, this routine was found to be significantly slower than polynomial approximations for `erfc` tabulated in Hart [13]. The particular polynomial approximations chosen from [13] for `erfc` are tables 5665 on  $[0, 2.5)$ , 5705 on  $[2.5, 5.5)$  and thirteen terms in the asymptotic expansion of the complimentary error function (from Abramowitz and Stegun [1]) on  $[5.5, \infty)$ . These polynomial approximations guarantee at least eleven digits of accuracy and an absolute error of less than  $10^{-15}$ , and are approximately seven times faster than the IMSL routine on a Sun Sparc 10.

To decide which of the Ewald and Poisson sum results to use for calculating  $G(\mathbf{R})$ , a computational comparison is made. The sums are calculated in layers as described in section 2.4 above until a relative error of  $10^{-8}$  is obtained. The Green's function is calculated for  $10^5$  cases at the points  $\mathbf{R} = (r \cos \theta, r \sin \theta)$ , where  $r = 0, 0.2, 0.4, \dots, 2$ , and  $\theta = 0, \pi/50, \pi/25, \dots, 2\pi$ , which spans the values of  $\mathbf{R}$  at which the Green's function needs to be calculated. The total time (in CPU seconds) needed to calculate the Green's function using the Ewald and Poisson sum results are compared, and for a particular

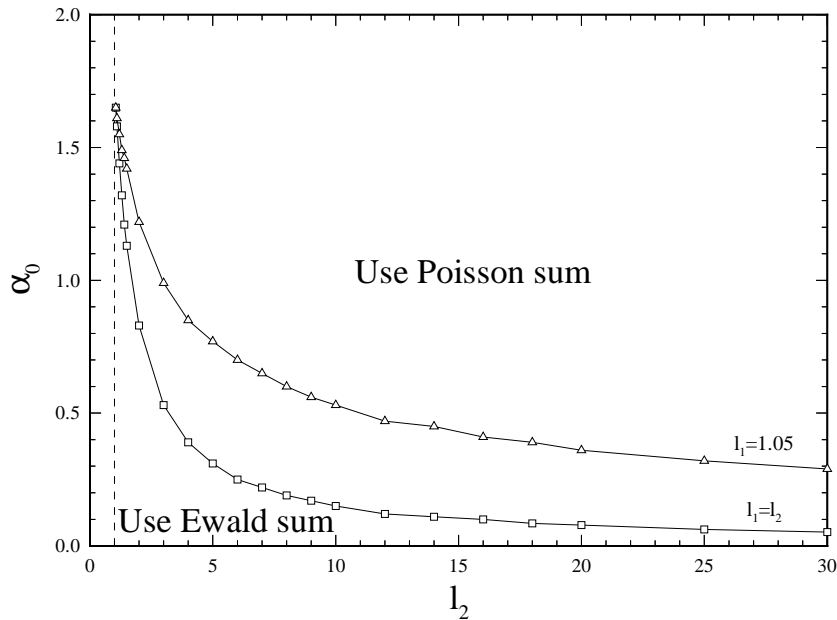


Figure 3: The value of  $\alpha$  at which the Poisson and Ewald summations take the same amount of CPU time versus  $l_2$  for the two cases  $l_1 = l_2$  and  $l_1 = 1.05$ . Above the curves the Poisson sum is more efficient, below the Ewald sum is superior.

$(l_1, l_2)$ , we can find a value  $\alpha_0$  such that when  $\alpha > \alpha_0$  the Poisson sum result (21) is more efficient, and when  $\alpha < \alpha_0$  the Ewald result is more efficient, and when  $\alpha = \alpha_0$  both results are equally good. For example, Figure 3 shows the curves of  $\alpha_0$  for the two cases  $l_1 = l_2$  and  $l_2 = 1.05$ , and indicates which of the Poisson or Ewald sums to use for a particular choice of  $\alpha$ . It should also be noted that the summations are significantly slower when the aspect ratio of the periodic cell gets large. For example, convergence for  $l_1 = 1.05, l_2 = 30$  is about 15 times slower than for  $l_1 = l_2 = 1.05$  at  $\alpha_0$ .

### 3 Solution Method and Numerical Details

We wish to solve the integral equation (9) where we choose the reaction parameters  $(\alpha, K)$ , and the periodic cell size parameters  $(l_1, l_2)$ . Depending on the parameters, we use data such as presented in Figure 3 to decide which form of the Green's function (21) or (31) to use. Since the electrode surface  $S_E$  is a disc of radius one, we have  $l_1, l_2 > 1$  so that the electrodes in the periodic array are not touching. As  $l_1, l_2$  become increasingly large, the solutions should approach that for a single disc on an insulating surface, as described in Bender and Stone [5]. Due to the problem geometry, it is natural to use a cylindrical coordinate system and so write

$$\int_{S_E} f(\mathbf{r}) dS(\mathbf{r}) = \int_0^1 \int_0^{2\pi} F(r, \theta) r d\theta dr, \quad (34)$$

where  $F(r, \theta) \equiv f(r \cos \theta, r \sin \theta)$ . Due to the symmetry of the problem, we only need to find  $\phi'$  in the first quadrant, and (9) can then be rewritten as

$$1 + \frac{1}{K} \phi'(r_0, \theta_0) = \int_0^1 \int_0^{\pi/2} 2\phi'(r, \theta) r \{G(r, \theta; r_0, \theta_0) + G(r, \pi - \theta; r_0, \theta_0) + G(r, \pi + \theta; r_0, \theta_0) + G(r, 2\pi - \theta; r_0, \theta_0)\} d\theta dr, \quad (35)$$

for  $0 \leq \theta_0 < \pi/2$ ,  $0 \leq r_0 < 1$ ,

where  $G(r, \theta; r_0, \theta_0) \equiv G(\mathbf{R}) = G(\mathbf{r} - \mathbf{r}_0)$  and we have explicitly written the unknown flux  $\phi'$  in polar coordinates.

To find the unknown flux  $\phi'$ , we divide the rectangle  $[0, 1] \times [0, \pi/2]$  in polar coordinates into  $M \times N$  elements, and assume that  $\phi'$  varies quadratically in  $r$  and  $\theta$ ; on the  $(i, j)$ th element, we assume  $\phi' = \sum_k \phi'_{ijk} N_k(\eta_1, \eta_2)$ , where  $(\eta_1, \eta_2)$  is the coordinate system for the  $(i, j)$ th element mapped onto  $[-1, 1] \times [-1, 1]$ ,  $N_k$  are the quadratic weight functions, and the  $\phi'_{ijk}$  are unknowns. By choosing the collocation points  $(r_0, \theta_0)$  to be the node points of the quadratic elements, we convert (35) to a linear system of equations for the  $\phi'_{ijk}$ , which can be solved by Gaussian elimination to obtain a solution for the flux. Further details on the quadratic element boundary element method can be found in standard boundary element texts such as Brebbia *et al.* [8].

### 3.1 Integration Techniques

The matrix elements in the linear system to be inverted involve two-dimensional integrals over the elements of the Green's function multiplied by the appropriate weight functions. If the current collocation point  $(r_0, \theta_0)$  is on the border or within the region we are integrating over, then there is a singularity in the function at that point, which must be handled more carefully. Here, we implement a scheme using 'degenerate quadrilaterals', originally described in Lachat and Watson [18]. If we transform a triangle onto a square, and stretch a corner of the triangle onto one of the square's sides, then the Jacobian of the transformation is such that a  $1/r$  singularity at the stretched corner of the triangle is removed, and no longer causes poor convergence for numerical integration rules. This idea is analogous to transforming a local cartesian coordinate system to polar coordinates with the origin at the singularity, and has the advantage that the degenerate quadrilateral transformation does not have to deal with circular arcs. An integration routine designed to integrate over a set of general quadrilaterals, given their four corners, thus has the advantage of being able to integrate over rectangular regions with no singularities (given the four corners) or deal with singularities in the region (divide into a set of triangles, with the singularity at a corner). Furthermore, the ability to integrate over a set of quadrilaterals is also useful in cases where elements have a high aspect ratio. For example, for long, thin integration regions, more function evaluations are usually required in the long direction to obtain suitable accuracy. It follows that, for the same accuracy, far fewer function evaluations are required if initially long thin regions are subdivided into smaller regions of lower aspect ratio. Numerical experiments performed here indicate that setting the maximum aspect ratio of a rectangle equal to 2 gives the best efficiency.

Another integration difficulty which arises in boundary integral calculations lies in choosing the order of the quadrature rule. Integrals over regions near the collocation point will typically require more effort than those far from it, but a simple distance rule is often insufficient, since the shape of the integration region is also important. Here, we use a combination of successive and adaptive quadrature rules in an attempt to produce a single integration routine to deal with the range of integrals required in a boundary element method. An initial approximation is made using  $4 \times 4$  and  $6 \times 6$  point Gauss-Legendre rules over general quadrilaterals, with an error estimate based on the difference between these rules. For a more detailed description of the error estimate, see Kahaner and Rechar [15]. If the error estimate is larger than that required, continue with  $8 \times 8$  and  $12 \times 12$  point rules. If the required accuracy has still not been obtained, use an adaptive method, where the quadrilateral with the largest error is subdivided into four new quadrilaterals, and the  $8 \times 8$  and  $12 \times 12$  point rules are applied to them. This adaptive process is continued until the estimated error is less than that requested. This combination of successive then adaptive algorithms has the advantage that it will not use a high order rule when not necessary (i.e. when the integration region is far from the collocation point), but will use efficient adaptive methods with reasonably high-order rules when required.

Finally, we note that evaluating the periodic Green's function (21) or (31) is substantially more expensive than evaluating the free space Green's function (22). Since for a quadratic boundary element method we integrate over each region for each collocation point eight times where the Green's function is multiplied by different weight functions, it makes sense to form all eight integrals one time, and use vector integration. In cases such as this where each of the integrands in the vector are very similar (different weight functions), substantial savings in time can be made by minimizing the number of times the Green's function has to be evaluated. For this problem a factor of 5 increase in speed of integration was obtained by changing from scalar to vector integration.

For the work described here, numerical integration is performed with a requested relative error of  $5 \times 10^{-6}$ , which guarantees at least 5 digits of accuracy.

## 3.2 Singularities in the Solution

Unfortunately, when the above procedures are used to solve the integral equation (35), the numerical solutions converge quite slowly as the number of quadratic elements is increased. The numerical inaccuracies arise because the function we are trying to find,  $\phi'$ , is itself poorly behaved as we approach the edge of the disc. The problem is qualitatively different in the two cases  $K = \infty$  and  $0 < K < \infty$ , which are now addressed separately.

### 3.2.1 The $K = \infty$ Case

In this case, the boundary conditions from (1) on  $z = 0$  become  $\phi = 1$  for  $\mathbf{r} \in S_E$  and  $\partial\phi/\partial z = 0$  for  $\mathbf{r} \in S_P$ . For the case of a single disc, not the periodic array, there is an exact analytic solution for the case  $\alpha = 0$ , the so-called 'electrified disc' solution (see for example Jackson [14] or Newman [21]), where the flux on the surface of the disc in

terms of radial position  $r$  is

$$\frac{\partial \phi}{\partial z} = -\frac{2}{\pi\sqrt{1-r^2}}. \quad (36)$$

The flux distribution has an inverse square root singularity at the edge of the disc,  $r = 1$ , which explains why a quadratic element approximation is relatively poor. This inverse square root singularity is common in problems where there is a change in boundary conditions, as is also the case in the stress field at a crack tip in classical elastostatics.

For the modified Helmholtz equation, analytic information on the leading term in the solution near the singularity can be found following the method described in Ramachandran [29] for Laplace's equation near the point where the boundary conditions suddenly change. We find that the leading order behavior near the edge  $x = 1 - r$  of  $\phi'$  is  $\phi' \propto I_{1/2}(\alpha x)xr$ , where  $I$  is the modified Bessel function of the first kind. For small  $x$  (near the singularity),  $\phi' \propto 1/\sqrt{x}$ , and so the form of the singularity is the same as for Laplace's equation, which is the modified Helmholtz equation with  $\alpha = 0$ . In fact, the solution has this inverse square root singularity in the flux  $\phi'$  regardless of the value of  $\alpha$  or whether we are dealing with a single or periodic array of electrodes. Thus, we replace  $\phi'(r, \theta)$  in the integral equation (35) by  $\hat{\phi}'(r, \theta)/\sqrt{1-r}$ , and solve for  $\hat{\phi}'$ . The inverse square root singular part of the flux is absorbed into the formulation, and the smooth contribution to the flux is all that remains to be approximated by the quadratic elements.

The additional  $1/\sqrt{1-r}$  term in the integral means that there is an additional singularity in the two-dimensional integrals over the elements whose edge corresponds to the edge of the disc. Transformations to remove endpoint algebraic singularities are available in Press *et al.* [28], and we make use of the identity

$$\int_{-1}^1 \frac{f(x)}{\sqrt{1-x}} dx = \int_{-1}^1 \sqrt{2}f\left(1 - \frac{1}{2}(1-t)^2\right) dt \quad (37)$$

to remove the square root singularity at  $r = 1$ .

The  $1/\sqrt{1-r}$  term also means that we cannot place collocation points at  $r_0 = 1$  (the edge of the disc). Normally, collocation points for quadratic elements are placed as shown in Figure 4a, where the element has been mapped onto  $[-1, 1] \times [-1, 1]$  in  $(\eta_1, \eta_2)$  space (Brebbia *et al.* [8]). For elements on the outer edge of the disc, we place collocation points as shown in Figure 4b. Collocation points previously at  $\eta_1 = 1$  have been moved to  $\eta_1 = 1/2$ .

### 3.2.2 The $K < \infty$ Case

Due to the boundary condition  $\phi = 1 + \phi'/K$  on the disc, there is no obvious way of analytically determining the form of the singularity in  $\phi'$  at the edge of the disc  $r = 1$ . The results for a single microelectrode in Bender and Stone [5] for finite  $K$  indicate  $\phi'$  is finite at  $r = 1$ , but has a derivative singularity, which becomes increasingly malignant as  $K$  increases. Since the solution is badly behaved at  $r = 1$ , we require more elements in the quadratic element discretization near the edge of the disc to increase accuracy with the same number of elements, rather than equally spaced as for the  $K = \infty$  case.

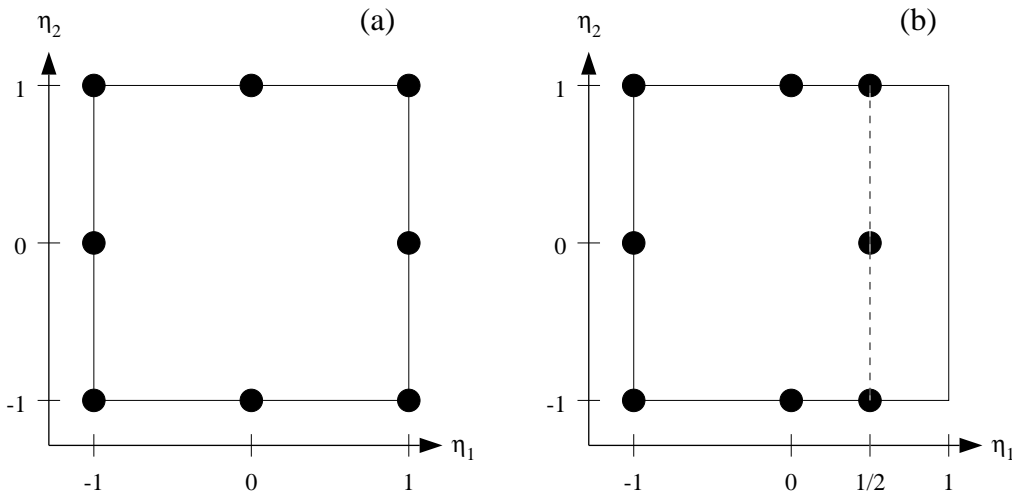


Figure 4: Positions of collocation points for a quadratic element transformed to  $(\eta_1, \eta_2)$  space, (a) normally and (b) when the element is on the edge of the disc, with the nodes positioned to avoid the inverse square root singularity at  $r = 1$ .

To this end, we place  $M/2$  elements in the  $r$  direction on  $r \in [0, 0.9]$  and  $M/2$  elements on  $r \in [0.9, 1]$ .

Figure 5 shows  $-\phi'$  versus  $r$  along  $\theta = 0^\circ$  for a single isolated electrode for the particular case  $\alpha = 10$ ,  $K = 100$ , and the non-equal spacing of elements. As the number of elements  $M$  in the radial direction increases, we can see the convergence of the curves to a final solution. Due to the derivative singularity in  $\phi'$  at  $r = 1$ , the quadratic element for  $-\phi'$  right near the edge has a concave up form. This numerical artifact is caused by fitting a quadratic to a curve with a singularity, and is particularly obvious for the  $M=8$  curve. This concave up behavior also occurs for the element just below  $r = 0.9$  as this is the radial value at which the width of elements suddenly changes.

While the detailed flux curves are poor for smaller numbers of elements, the solutions for total flux over the disc from (2), as shown in Table 1 converge significantly faster. For  $N=16$ , the flux curve is inaccurate enough to be easily seen by the naked eye, and yet the total flux result has three digits of accuracy. This result occurs regularly in boundary integral research; the calculated solution may be quite poor, but integrated results are more accurate. Since we are more interested in the flux per disc rather than the flux at a particular point on the disc, calculations on non-equally spaced elements will be used for finite  $K$ .

## 4 Results

Numerical results are reported first for  $K = \infty$  and then for finite  $K$ . We note that the periodic formulation as given here breaks down in the cases  $\alpha = 0$ . This is the limit of no bulk species regeneration, and all reactants at the electrodes are supplied by diffusion. In the single disc case (Bender and Stone [5]), the flux was easily calculated, but the infinite sum for the periodic Green's function tends to infinity as  $\alpha \rightarrow 0$ . This is due to

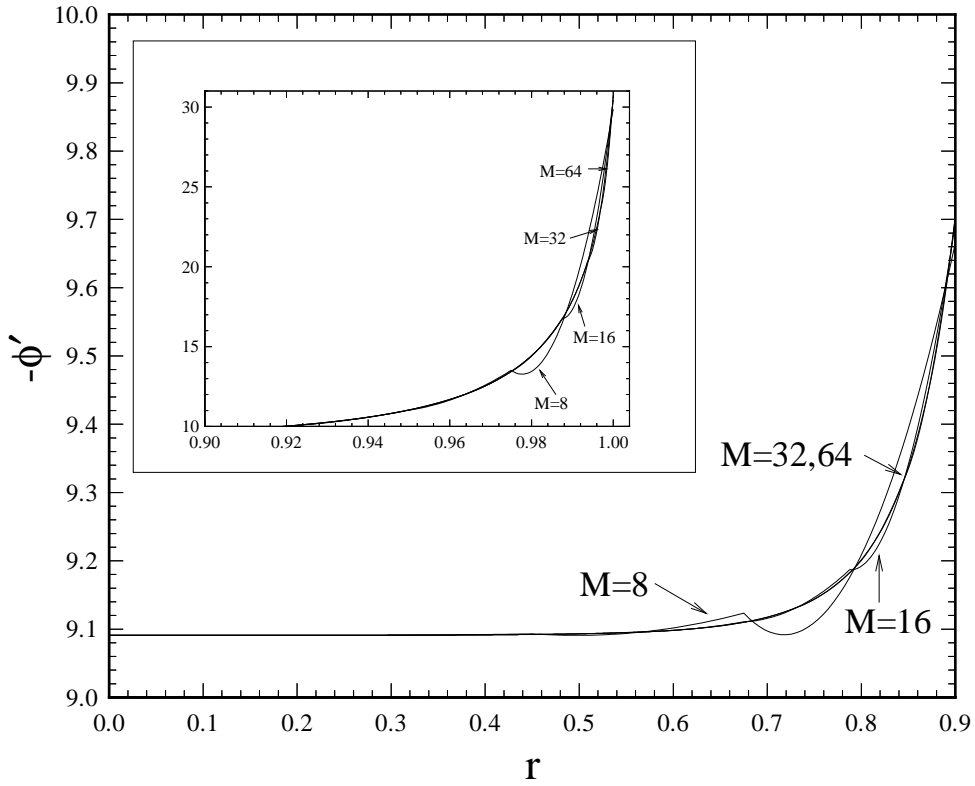


Figure 5:  $-\phi'$  versus  $r$  for  $\theta = 0^\circ$  for a single microelectrode, varying the number of elements. The parameters are  $\alpha = 10$ ,  $K = 100$ , and curves are for various numbers of elements in the  $r$  direction. The larger graph shows  $-\phi'$  on  $r \in [0, 0.9]$ , with the inset showing the results on  $r \in [0.9, 1]$ .  $M$  represents the number of elements in the  $r$  direction for the different solutions.

M	Total flux
2	31.548071
4	31.042502
8	30.942839
16	30.919375
32	30.914033
64	30.912789

Table 1: Convergence of the total flux for a single disc with  $\alpha = 10$  and  $K = 100$  as the number of unknowns is increased.  $M$  is the number of quadratic elements in the  $r$ -direction.

the denominator of (15) tending to zero as  $\alpha$  tends to zero for the term  $m_1 = m_2 = 0$ . In fact, as  $\alpha \rightarrow 0$ , the flux through each electrode in the periodic array goes to zero. In the single electrode case, diffusion can bring reactants to the electrode from the entire space  $z > 0$ , and it is possible to have a nonzero flux on the disc as  $\phi$  and  $\phi'$  go to zero at infinity. For the periodic array, each electrode can only absorb reactants diffused from the volume above its own periodic cell in the  $\alpha = 0$  case, and since  $\phi' = 0$  at  $z = \infty$ , the ‘top’ of the periodic volume, conservation implies that there is no flow of reactants, and the flux goes to zero. Thus, while no results can be calculated for the periodic problem with  $\alpha = 0$ , there can be assumed to be a zero flux, regardless of  $K$ , as long as  $l_1$  and  $l_2$ , the periodic cell size parameters, are finite. While there are a set of problems where there is a nonzero concentration gradient at infinity, the current formulation cannot deal with such a case, and is beyond the scope of this paper.

It should also be noted that by changing the Green’s function to the free-space form (22), the quadratic boundary element method described above can be used to reproduce the results of Bender and Stone [5] for a single disc on an insulating surface. In all cases, the different numerical implementations gave identical results to the reported accuracies.

#### 4.1 Results for $K = \infty$

We present first the results for the case of instantaneous reaction at the electrode surface, the limit  $K = \infty$ . The assumption of an inverse square root singularity in the solution described in section 3.2.1 above was successful for all these cases. We found that  $5 \times 5 = 25$  elements are sufficient to give flux results which are almost indistinguishable from higher order discretizations, and the results for total flux through an electrode, calculated using (2), are accurate to at least 3 digits. The accuracy is highest for small  $\alpha$ , up to 6 digits, and diminishes as  $\alpha$  increases, owing to the formation of boundary layers with large gradients.  $5 \times 5$  quadratic elements produce a linear system of equations with 96 unknowns, for which the solution with  $l_1 = l_2$  takes 10 minutes of CPU time on a Sun Sparc 10 workstation. For periodic cells with  $l_1 \neq l_2$ , the computation times can be much longer – up to 150 minutes for  $l_1 = 1.05$  and  $l_2 = 30$ , for example.

We first show the  $\theta$ -dependence of the flux  $\phi'$ . Figure 6 plots  $-\phi'$  as a function of  $r$ ,  $\theta$  for the parameters  $\alpha = 0.01$ ,  $K = \infty$  and  $l_1 = l_2 = 1.05$  in the first quadrant. On the diagonal  $\theta = 45^\circ$ , the flux takes its maximum value. This response is expected, since the distance to the nearest disc is highest at this angle.

Figure 7 shows the total flux per disc as a function of  $l_1 = l_2$  for various values of  $\alpha$ ; Figure 7(b) is a magnification of the dotted rectangle in Figure 7(a). The horizontal dashed lines in Figure 7(a) represent the results for a single disc on the insulating surface, while the vertical line in Figure 7(b) at  $l_1 = l_2 = 1$  indicates where electrodes touch. Figure 8 shows this information by plotting flux per disc versus  $\alpha$  for various values of  $l_1 = l_2$ . Not surprisingly, as  $l_1 = l_2$  increase in size, the flux per disc approaches that for a single disc. As  $\alpha$  increases, the approach to the single disc result is much more rapid. Not plotted in Figure 7 are results for  $\alpha = 5$ , where the single disc flux is 18.9931 and for  $l_1 = l_2 = 1.05$  the flux per disc is 18.1444. Even more extreme are the results for  $\alpha = 10$ , where the single disc flux is 34.6453 and for  $l_1 = l_2 = 1.05$  the

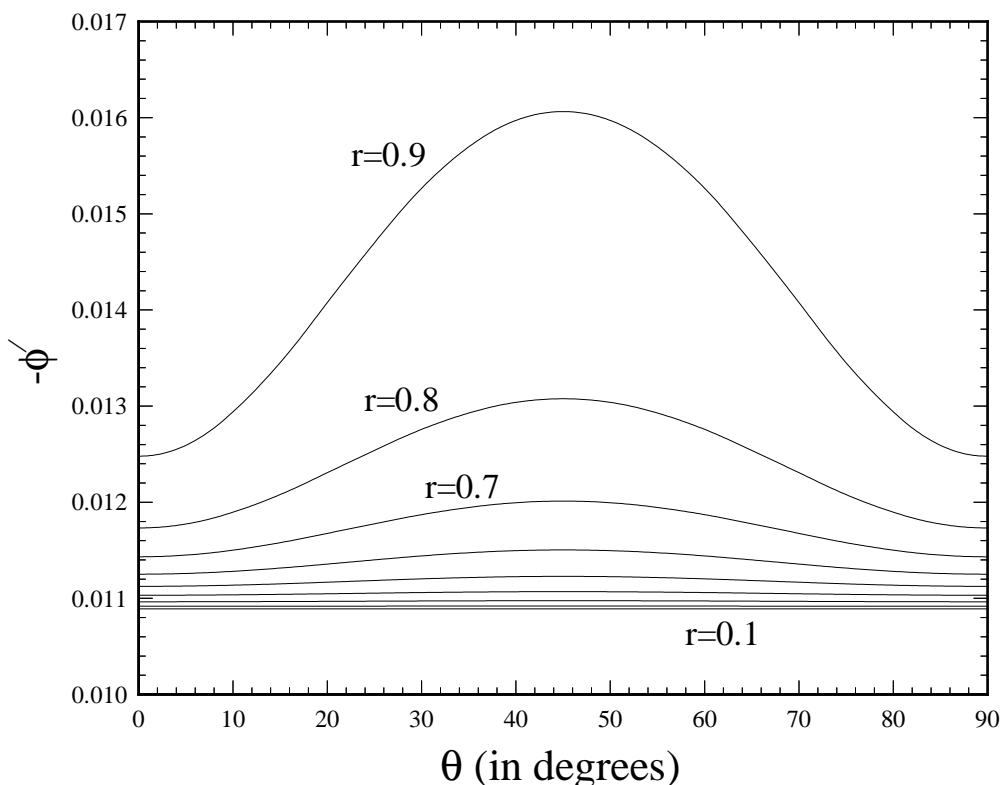


Figure 6: Plots of  $-\phi'$  versus  $\theta$  for  $r = 0.1, 0.2, \dots, 0.9$ ;  $\alpha = 0.01$ ,  $K = \infty$ ,  $l_1 = l_2 = 1.05$ .

flux per disc is 34.3020. We only have to increase the spacing to  $l_1 = l_2 = 1.5$  before the flux per disc results for  $\alpha = 10$  are identical to six figures to those for the single disc. Physically, for large  $\alpha$ , bulk regeneration of reactants within the fluids is large with respect to diffusion, and so most reaction occurs close to the electrode. As  $\alpha$  increases, the region of reaction around the electrode decreases, and so the distance over which individual electrodes have an effect on each other decreases. For small  $\alpha$ , on the other hand, diffusion dominates, and the restriction of each electrode only having access to the reactants in the fluid above its own periodic cell becomes more important. We can see in Figure 8 that for small  $\alpha$ , even for large values of  $l_1 = l_2$ , the flux per disc is significantly below the single disc result. The influence of electrodes on their neighbors is far more dramatic when diffusion dominates.

From the standpoint of design it is more important to evaluate the average flux per unit area of the bounding surface. This information is easily obtained as the flux per disc divided by the area of the periodic cell, and is plotted in Figure 9 as a function of  $l_1 = l_2$  for various  $\alpha$ . The flux per unit area provides a better indication of the overall transport properties of the periodic array, since it is a measurement that has scaled out the periodic cell size. The results show that for large  $l_1 = l_2$ , the slope of the curves is  $-2$ . Since for large  $l_1 = l_2$  the flux per disc approaches a constant (the single disc result), we have the same flux per periodic cell when the cell size increases. Since the area of the periodic cell increases as the square of the cell lengths, the factor of  $-2$  is as expected. We have also included in Figure 9 a dotted line across the various  $\alpha$  curves as

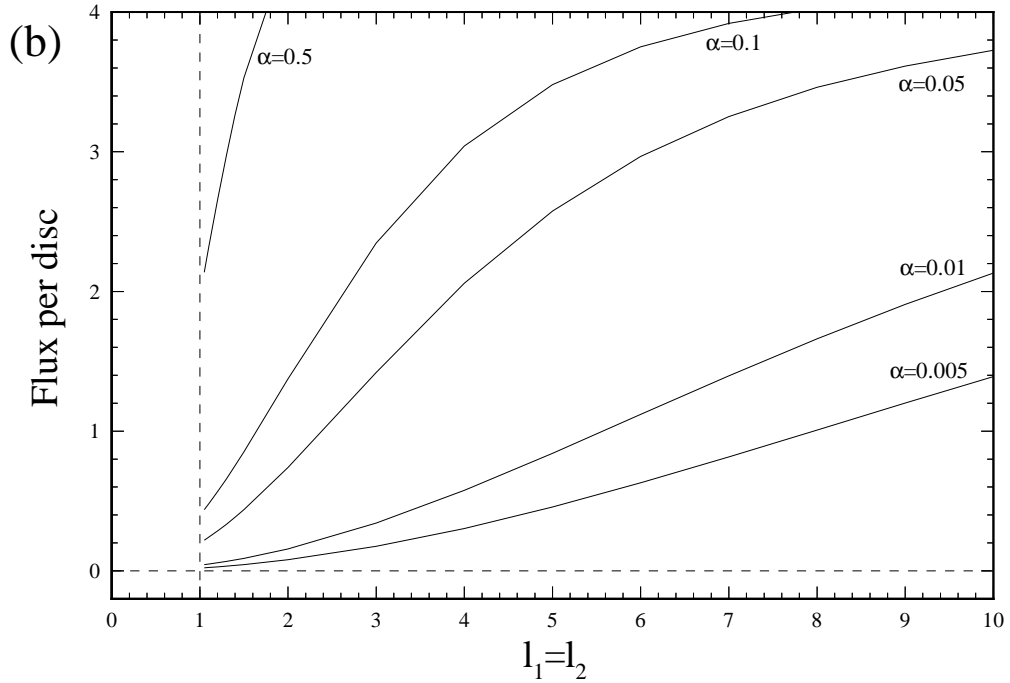
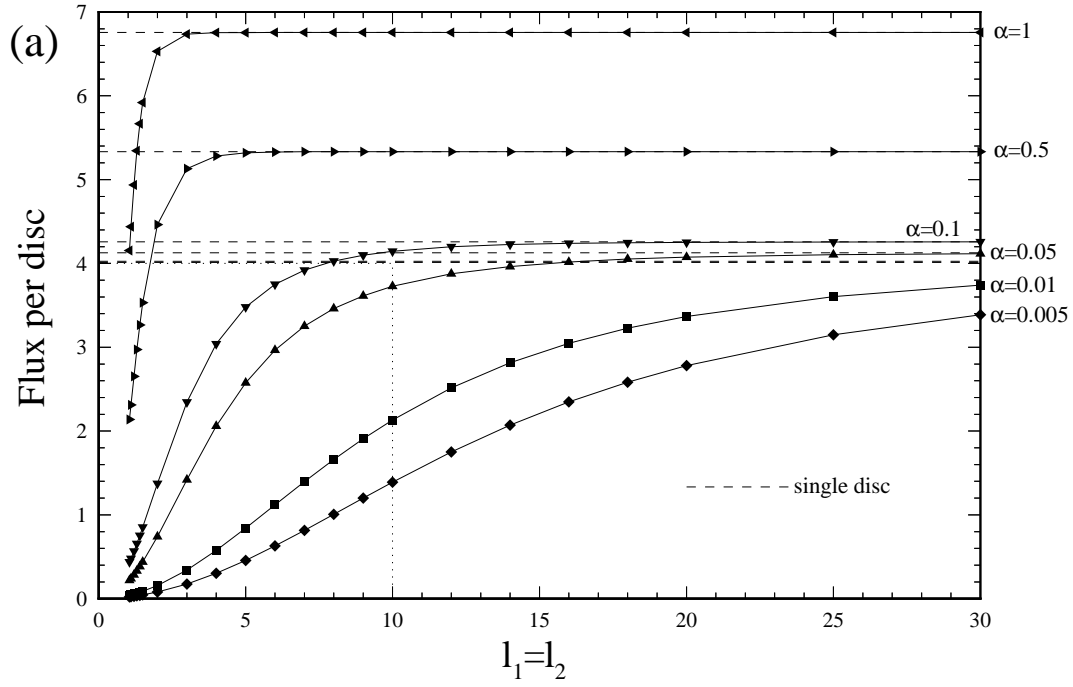


Figure 7: Flux per disc versus  $l_1 = l_2$  for various values of  $\alpha$  and  $K = \infty$ . The graph (b) enlarges the dotted rectangle in (a). The vertical line at  $l_1 = l_2 = 1$  indicates the point at which discs would touch.

a measure of the effectiveness of close-packing the electrodes on the insulating surface. The dotted line is the value of  $l_1 = l_2$  at which the flux per unit area is 90% of its value at  $l_1 = l_2 = 1.05$ , and we can see that as  $\alpha$  decreases, this value increases. It is thus evident that placing electrodes closer together yields a much smaller additional increase in flux for small  $\alpha$ . Since placing electrodes closer together is presumably more expensive in terms of time and materials, a point may be reached where placing electrodes closer together is uneconomical. This argument is even more important if the catalytic analog of this problem is considered, in which case the flux relates to the total reaction in the system due to catalytic sites, which we may be trying to maximize.

We also include here comparisons of the variation of  $\phi'$  with respect to angle  $\theta$  as the size of the periodic cell increases. Figure 10 shows curves of flux divided by its minimum value for  $\alpha = 0.01$ ,  $r = 0.9$ ,  $\theta$  in the first quadrant, and varying the periodic cell size. The curves have been scaled by the values of the flux at  $r = 0.9$  and  $\theta = 0^\circ$ , so that the variations are emphasised. Table 2 reports the values of the flux at  $r = 0.9$  and  $\theta = 45^\circ$  for the various periodic cell sizes, and shows the percentage variation between maximum and minimum  $\phi'$  values. We see that the percentage variation is decreasing more rapidly with increasing periodic cell size than the convergence of the  $\phi'_{min}$  values. In fact, the flux per disc results from Figure 7 show that, for  $\alpha = 0.01$ , the flux per disc is still well below the single disc flux for  $l_1 = l_2 = 30$ , which indicates that the variation of  $\phi'$  with  $\theta$  is only due to the close proximity of the electrodes for small  $l_1, l_2$ . For moderate to large spacings, the discs are far enough away from each other to cause minimal disturbances in their neighbor's flux, but the limitations on volume available for diffusion (only the volume above the periodic cell for each electrode) result in the low flux per disc. In fact, this observation explains the observable point of inflexion in the curves of flux per disc for  $\alpha = 0.1, 0.05, 0.01, 0.05$  shown earlier in Figure 7(a). There is a drop in flux per disc as  $l_1 = l_2$  decreases due to the reduced size of the periodic cell. However, as  $l_1 = l_2$  gets small enough, there is additional interaction between the discs themselves, causing the angular variation of  $\phi'$  observed in Figure 10.

Finally, in Figure 11, the flux per disc is shown with curves for different  $\alpha$ , but now  $l_1 = 1.05$  always, and  $l_2$  is varied, thus increasing the aspect ratio of the periodic cell. For large  $l_2$ , this geometry will look like widely separated parallel rows of discs. We see that the convergence to a set flux per disc as  $l_2$  increases is about the same as for the  $l_1 = l_2$  case. However, the value the flux per disc converges to is reduced, by a greater fraction as  $\alpha$  gets smaller. We also see that the inflexion in the curves in Figure 7(a) are not seen in Figure 11. Since  $l_1 = 1.05$ , discs will always be close together in the  $x$  direction, and so the change in behavior as discs get further apart is not apparent here.

## 4.2 Results for Finite $K$

For finite  $K$ , tests were performed for the single microelectrode case for various  $\alpha$  and  $K$  with nonequally spaced elements in the radial direction. It was found that 3-6 digits of accuracy in the total flux are obtained using  $M=16$  elements (8 on  $r \in [0, 0.9]$ , 8 on  $r \in [0.9, 1]$ ), with the accuracy highest for small  $K$ . Thus, results quoted here used  $16 \times 5 = 80$  element discretizations.  $16 \times 5$  quadratic elements lead to 283 unknowns, and solution took roughly three hours on a Sun Sparc 10. It should also be noted that

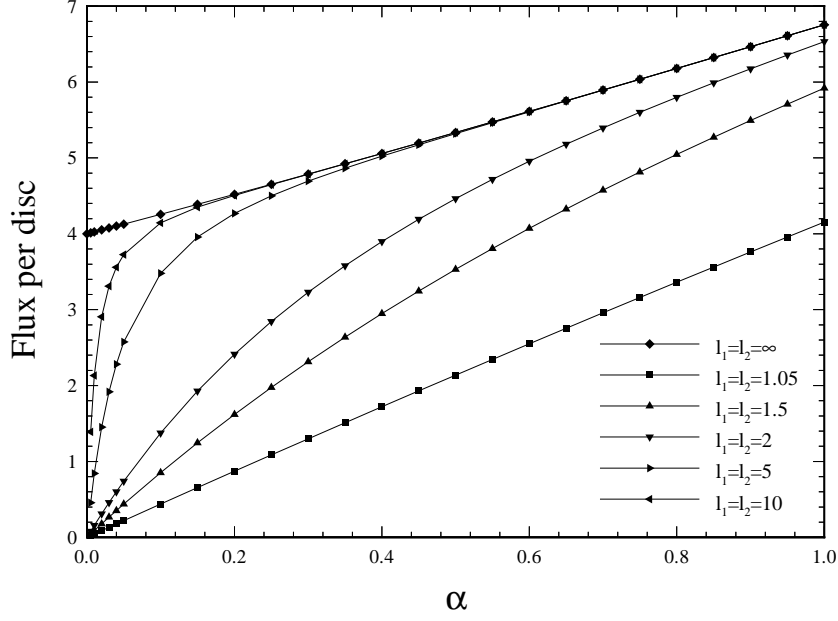


Figure 8: Flux per disc versus  $\alpha$  for various values of  $l_1 = l_2$  and  $K = \infty$ .

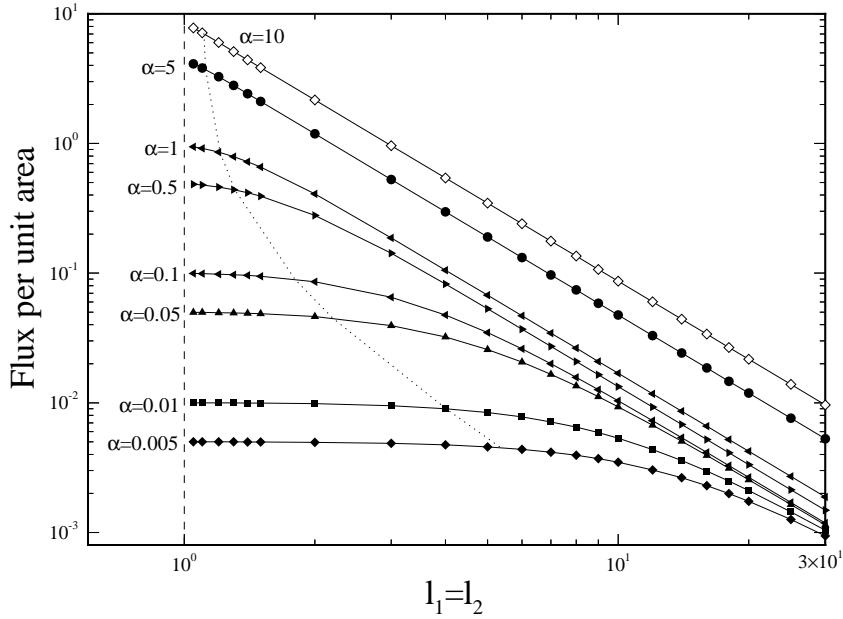


Figure 9: Flux per unit area versus  $l_1 = l_2$  for various values of  $\alpha$  and  $K = \infty$ . The dotted line represents the value of  $l_1 = l_2$  at which the flux per unit area is 90% of its value at  $l_1 = l_2 = 1.05$ .

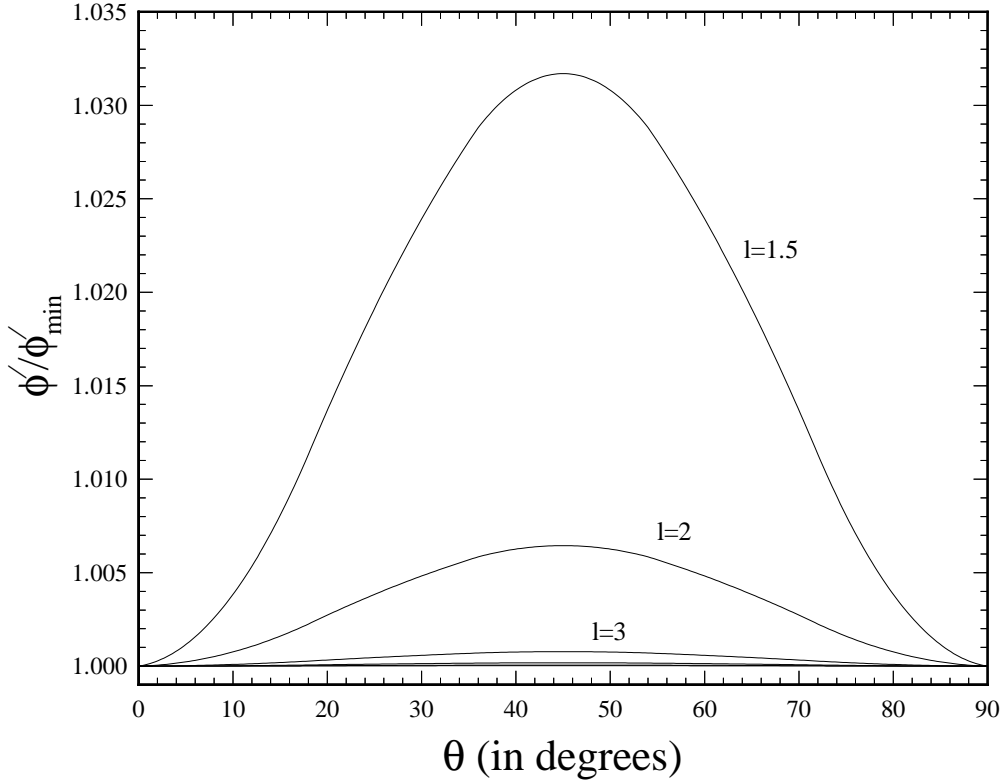


Figure 10: Flux curves divided by their minimums versus  $\theta$  along  $r = 0.9$ ;  $\alpha = 0.01$ ,  $K = \infty$ , and  $l_1 = l_2 = 1.05, 2, 3, 4, 5, 6$ .

$l_1 = l_2$	$\phi'_{min}$	% Variation
1.05	$-3.105 \times 10^{-2}$	3.1
2	$-5.650 \times 10^{-2}$	0.64
3	$-1.242 \times 10^{-1}$	0.077
4	$-2.100 \times 10^{-1}$	0.018
5	$-3.070 \times 10^{-1}$	0.0058
6	$-4.087 \times 10^{-1}$	0.0023

Table 2: For each  $l_1 = l_2$ ,  $\phi'_{min}$  represents the minimum value of  $\phi'$  for  $r = 0.9$ , which is at  $\theta = \pi/4$ . The third column holds the percentage variation between maximum and minimum values of  $\phi'$ .

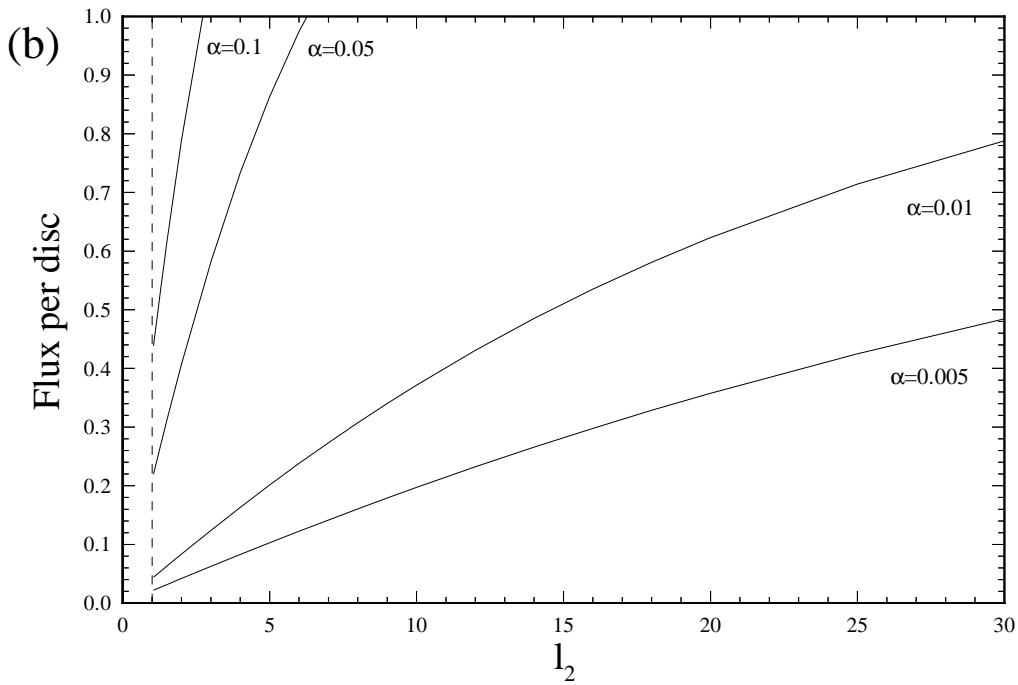
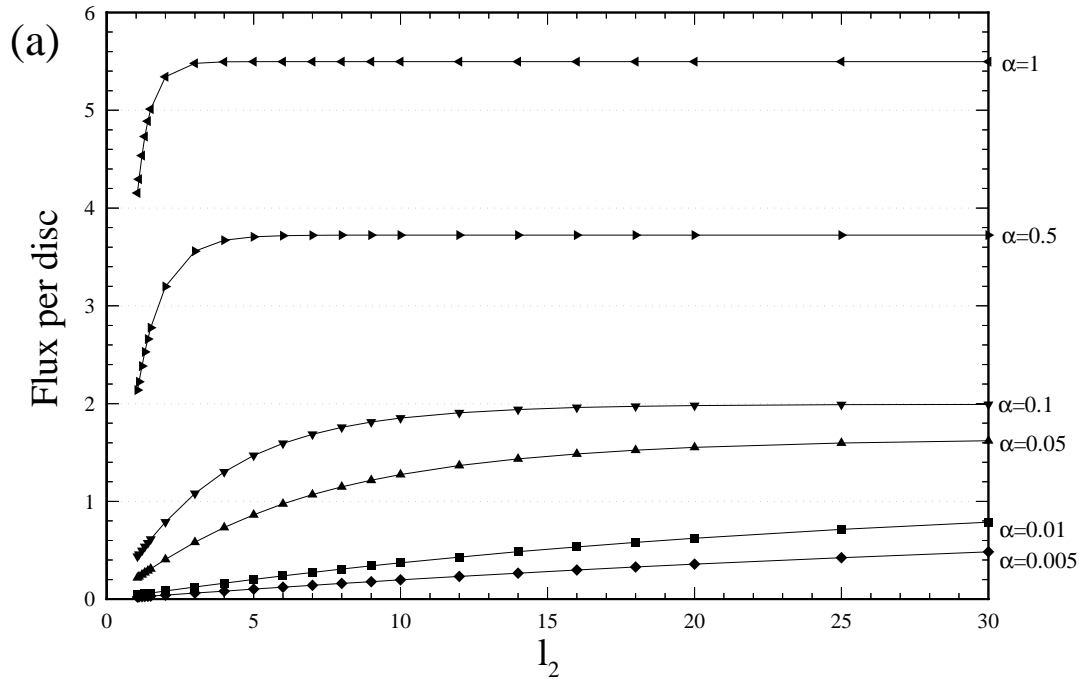


Figure 11: Flux per disc versus  $l_2$  for  $l_1 = 1.05$  and various values of  $\alpha$ . Graph (b) is an expansion of the lower section of (a).

the integral terms from (35) are independent of  $K$ , and so calculations for a particular  $\alpha$ ,  $l_1$ , and  $l_2$  can be used for various  $K$  with minimal extra calculation - just the inversion of a matrix.

With the enormous range of parameters available, we choose to present in Figure 12 the flux per disc versus  $l_1 = l_2$  results for  $\alpha = 0.01$  and  $\alpha = 0.5$  for various  $K$ . The results for  $K = \infty$  from Figure 7 are included to show the upper bounds on the possible flux per disc in these cases. For small  $K$ , the curves of flux per disc versus  $l_1 = l_2$  reach a steady state more quickly than for higher  $K$ . We can also see that for  $K > 100$ , there is very little difference in flux per disc compared to the  $K = \infty$  case. If for physical systems there is a cost involved in increasing the surface reaction rate  $K$  of the electrodes, then there is a break even point at which increases in  $K$  result in increases in flux per disc that are uneconomical. Also, for particular  $\alpha$ ,  $l_1$ ,  $l_2$ , a value of  $K$  can be found at which the flux per disc is any given percentage of the  $K = \infty$  result.

## 5 Conclusion

Bender and Stone [5] developed an integral equation approach to the single disc steady state microelectrode problem, and produced results of greater accuracy and flexibility (e.g. not limited to the pure diffusion,  $\alpha = 0$ , case) than previously available. A combined eigenfunction expansion and boundary collocation approach was recently described by Fransaer *et al.* [11], who also treated a finite number of electrodes. Here, we have extended those results to the periodic microelectrode problem, and have investigated the effects of varying the periodic cell size. By allowing the flux  $\phi'$  to vary in both  $r$  and  $\theta$  directions and using a periodic Green's function, we have obtained results for periodic systems, and have obtained results over a range of  $\alpha$  and  $K$  values.

There are a number of possible simple extensions of the techniques presented here for further analysis. The problem of a ring microelectrode, or indeed any other potentially interesting shape, can be modelled in both the single and periodic cases. For situations where we wish to maximize the flux per unit area from a periodic array, while minimizing the quantity of microelectrode material placed on the plane, ring electrodes may indeed be more useful than discs. Also, the problem of random positioning of microelectrodes on a surface may be simulated by a periodic cell containing a random collection of microelectrodes, random in both position and/or size.

### Acknowledgments

We gratefully acknowledge NSF-PYI Award CT5-8957043 (to HAS) and the MERCK Foundation for funding this study. We thank Professors Ali Nadim and Ashok Sangani for helpful conversations and discussions concerning Ewald sums. We would also like to thank the referees for their helpful suggestions. This research was undertaken when SKL was a postdoctoral research fellow at Harvard University, under HAS.

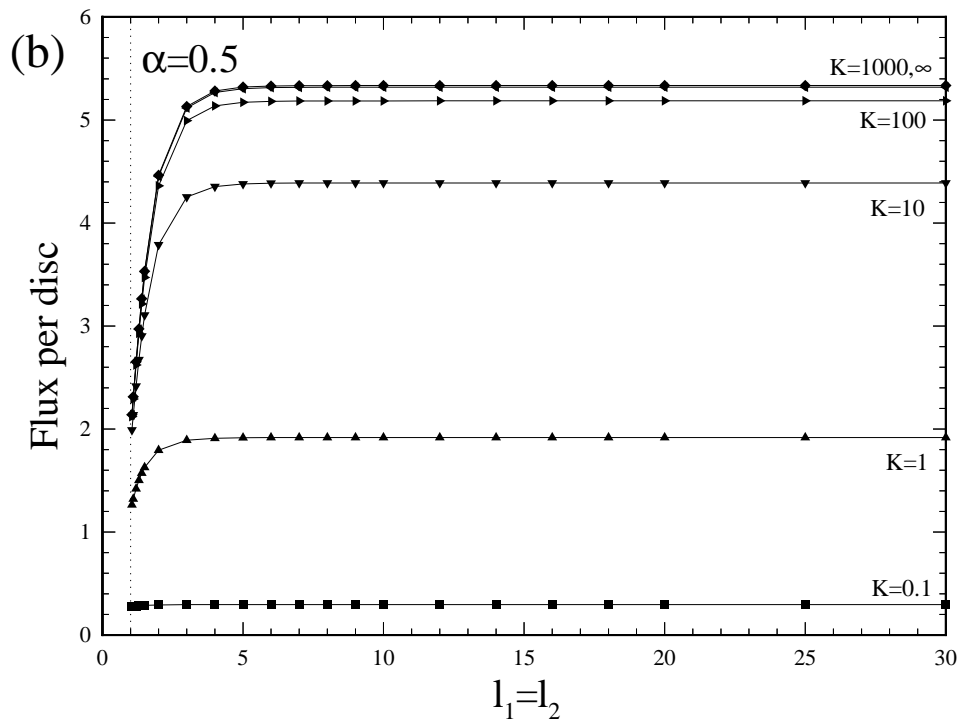
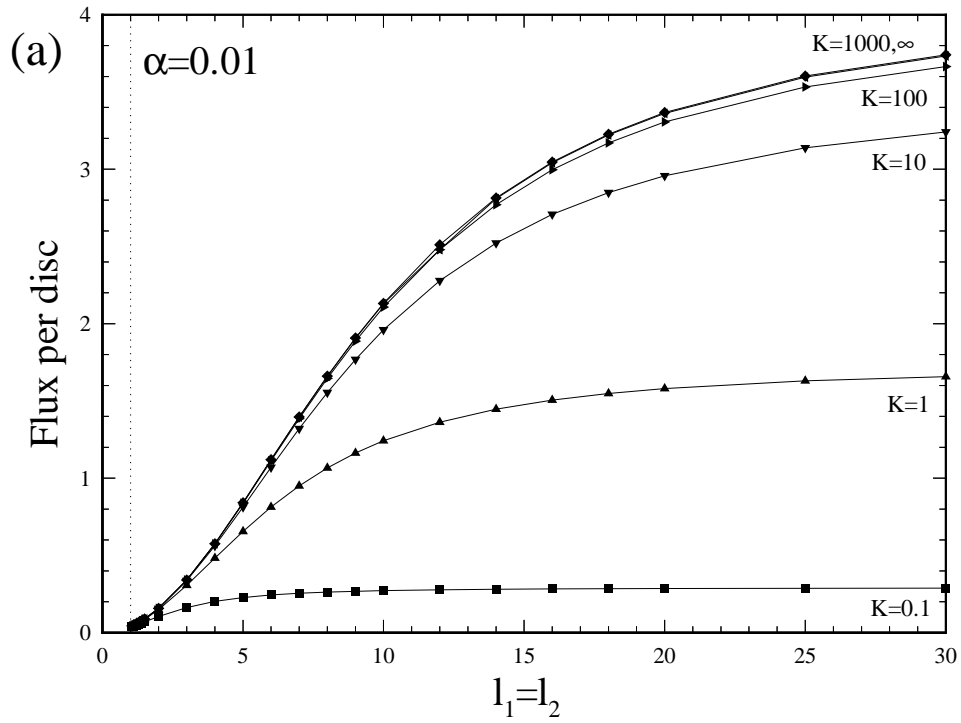


Figure 12: Flux per disc versus  $l_1 = l_2$  for various values of  $K$  and (a)  $\alpha = 0.01$  and (b)  $\alpha = 0.5$ .

# References

- [1] M. Abramowitz and I. A. Stegun, *Handbook of Mathematical Functions*, Dover, New York, 1972.
- [2] K. Aoki, K. Tokuda and H. Matsuda, *Theory of stationary current-potential curves at microdisk electrodes for quasi-reversible and totally irreversible electrode reactions*, J. Electroanal. Chem., 235 (1987), pp. 87–96.
- [3] G. Balgi, D.E. Leckband and J.M. Nitsche, *Transport effects on the kinetics of protein-surface binding*, preprint, 1995.
- [4] G. Barton, *Elements of Green's Functions and Propagation*, Oxford University Press, 1989.
- [5] M.A. Bender and H.A. Stone, *An integral equation approach to the study of the steady state current at surface microelectrodes*, J. Electroanal. Chem., 351 (1993), pp. 29–55.
- [6] A.M. Bond, K.B. Oldham and C.G. Zoski, *Theory of electrochemical processes at an inlaid microelectrode under steady-state conditions*, J. Electroanal. Chem., 245 (1988), pp. 71–104.
- [7] R.T. Bonnecaze and J.F. Brady, *A method for determining the effective conductivity of dispersions of particles*, Proc. R. Soc. Lond. A, 430 (1990), pp. 285–313.
- [8] C.A. Brebbia, J.C.F. Telles and L.C. Wrobel, *Boundary Element Techniques: Theory and Applications in Engineering*, Springer-Verlag, Berlin, 1984.
- [9] M. Fleischmann, S. Bandyopadhyay and S. Pons, *The behaviour of microring electrodes*, J. Phys. Chem., 89 (1985), pp. 5537–5541.
- [10] M. Fleischmann and S. Pons, *The behaviour of microdisk and microring electrodes*, J. Electroanal. Chem., 222 (1987), pp. 107–115.
- [11] J. Fransaer, J.P. Celis and J.R. Roos, *Variations in the flow of current to disk electrodes caused by particles*, J. Electroanal. Chem., 391 (1995), pp. 11–28.
- [12] I.S. Gradshteyn and I.M. Ryzhik, *Table of Integrals, Series and Products*, Academic Press, Boston, 5th ed., 1994.
- [13] J.F. Hart, *Computer Approximations*, Wiley, New York, 1968.
- [14] J.D. Jackson, *Classical Electrodynamics*, Wiley, New York, 1962.
- [15] D.K. Kahaner and O.W. Rechar, *TWODQD an adaptive routine for two-dimensional integration*, J. Comp. Appl. Math., 17 (1987), pp. 215–234.
- [16] D.-Y. Kuan, H.T. Davis and R. Aris, *Effectiveness of catalytic archipelagos. I regular arrays of regular islands*, Chem. Eng. Science, 38 (1983), pp. 719–732.
- [17] D.-Y. Kuan, R. Aris and H.T. Davis, *Effectiveness of catalytic archipelagos. II random arrays of random islands*, Chem. Eng. Science, 38 (1983), pp. 1569–1579.
- [18] J.C. Lachat and J.O. Watson, *Effective numerical treatment of boundary integral equations: a formulation for three-dimensional elastostatics*, Int. J. num. Meth. Eng., 10 (1976), pp. 991–1005.
- [19] T.E. Mallouk, *Minituarized electrochemistry*, Nature, 343 (1990), pp. 515–516.

- [20] S.J. Miklavic, D.Y.C. Chan, L.R. White and T.W. Healy, *Double layer forces between heterogeneous charged surfaces*, J. Phys. Chem., 98 (1994), pp. 9022–9032.
- [21] J. Newman, *Resistance for flow of current to a disk*, J. Electrochem. Soc., 112 (1966), pp. 501–502.
- [22] B.R.A. Nijboer and F.W. De Wette, *On the calculation of lattice sums*, Physica, 23 (1957), pp. 309–321.
- [23] K.B. Oldham and C.G. Zoski, *Comparisons of voltammetric steady states at hemispherical and disc microelectrodes*, J. Electroanal. Chem., 256 (1988), pp. 11–19.
- [24] C.G. Phillips, *The steady-state current for a microelectrode near diffusion-limited conditions*, J. Electroanal. Chem., 291 (1990), pp. 251–256.
- [25] C.G. Phillips, *The steady, diffusion-limited current at a disk microelectrode with a first order EC' reaction*, J. Electroanal. Chem., 296 (1990), pp. 255–258.
- [26] C.G. Phillips, *The steady current for monticulate microelectrodes and assemblies of ultramicroelectrodes*, J. Electrochem. Soc., 139 (1992), pp. 2222–2230.
- [27] C.G. Phillips and H.A. Stone, *The steady-state current for a ring-like microelectrode under non-diffusion-controlled conditions*, J. Electroanal. Chem., to appear (1995).
- [28] W.H. Press, B.P. Flannery, S.A. Teukolsky and W.T. Vetterling, *Numerical Recipes: The Art of Scientific Computing*, Cambridge University Press, 1989.
- [29] P.A. Ramachandran, *Boundary Element Methods in Transport Phenomena*, Computational Mechanics Publications, Southampton, 1994.
- [30] H. Reller, E. Kirowa-Eisner and E. Gileadi, *Ensembles of microelectrodes, a digital simulation*, J. Electroanal. Chem., 138 (1982), pp. 65–77.
- [31] A.S. Sangani and R. Sureshkumar, *Linear acoustic properties of bubbly liquids near natural frequency of bubbles using numerical simulations*, J. Fluid Mech., 252 (1993), pp. 239–264.
- [32] B.R. Scharifker, *Diffusion to ensembles of microelectrodes*, J. Electroanal. Chem., 240 (1988), pp. 61–76.
- [33] A. Szabo, *Theory of the current at microelectrodes, applications to ring electrodes*, J. Phys. Chem., 91 (1987), pp. 3108–3111.
- [34] P.W. Voorhees and M.E. Glicksman, *Solution to the multi-particle diffusion problem with applications to Ostwald ripening - I. theory*, Acta metall., 32 (1984), pp. 2001–2011.
- [35] R.M. Wightman and D.O. Wipf, *Voltammetry at ultramicroelectrodes*, Electroanal. Chem., 15 (1989), pp. 267–353.
- [36] IMSL MATH/LIBRARY Special Functions Version 2.0 (FORTRAN subroutines for mathematical applications), IMSL, Houston, 1991.